SLOVAK UNIVERSITY OF TECHNOLOGY
IN BRATISLAVA

FACULTY OF CHEMICAL AND FOOD TECHNOLOGY

Reg. No.: FCHPT-5431-82597

Modelling and Optimisation of Membrane Process Operation

BACHELOR THESIS

2018 Lukáš Šatura

SLOVAK UNIVERSITY OF TECHNOLOGY IN BRATISLAVA

FACULTY OF CHEMICAL AND FOOD TECHNOLOGY

Reg. No.: FCHPT-5431-82597

Modelling and Optimisation of Membrane Process Operation

BACHELOR THESIS

Study Programme:	Chemical Engineering
Study Field:	5.2.17. Chemical Engineering
Training Workplace:	Institute of Information Engineering, Automation, and Mathematics
Thesis Supervisor:	doc. Ing. Radoslav Paulen, PhD.

Bratislava 2018 **Lukáš Šatura**

Slovak University of Technology in Bratislava
Institute of Information Engineering, Automation and Mathematics

Faculty of Chemical and Food Technology
Academic year: 2017/2018
Reg. No.: FCHPT-5431-82597

STU FCHPT

BACHELOR THESIS TOPIC

Student: **Lukáš Šatura**
Student's ID: 82597
Study programme: Chemical Engineering
Study field: 5.2.17. Chemical Engineering
Thesis supervisor: doc. Ing. Radoslav Paulen, PhD.

Topic: **Modelling and Optimisation of Membrane Process Operation**

Language of thesis: English

Specification of Assignment:

Membrane separation is on of the most modern and most profitable separation techniques in chemical and biochemical industry. The goal of this project is to create a mathematical model of a laboratory plant for membrane separation, to estimate parameters of the model based on measured data, to verify correctness of the created model on a real plant, and to design an optimal operation of the plant.

Selected bibliography:

1. Mulder, M. *Basic Principles of Membrane Technology.* Dordrecht : Kluwer Academic Publishers, 1991. 363 s. ISBN 0-7923-0978-2.
2. Paulen, R. – Fikar, M. *Optimal Operation of Batch Membrane Processes.* Cham: Springer, 2016. 158 s. ISBN 978-3-319-20474-1.

Assignment procedure from: 12. 02. 2018
Date of thesis submission: 06. 05. 2018

Lukáš Šatura
Student

prof. Ing. Miroslav Fikar, DrSc.
Head of department

prof. Ing. Ľudovít Jelemenský, DrSc.
Study programme supervisor

To Mom...

...and Dad, siblings Tomáš and Gabriela; then to Barborka, Vanessa, Tomáš, Hana, Andrej, Han, Mika, Rafael and others, for your priceless support, professional guidance, inspiration, coffee, pancakes, and late-lunch conversations during my Bachelor's studies.

This thesis is built on experimental measurements thanks to the selfless attitude of Richard[1], who produced 429 L of RO-water. The greatest share of gratitude is dedicated to Radoslav[2]—who devoted over 71 hours on thesis supervision—for all intense consultations, laboratory visits, and valuable comments.

[1] Ing. Richard Valo, PhD.
[2] Thesis Supervisor

Abstract

Optimisation of any membrane diafiltration unit operation is vital for processing large feed volumes, as long as the overall process time and water consumption are concerned. Among others, also in separation processes of food and pharmaceutical industry. Besides correct estimation of fundamental parameters of filtration system, model of transmembrane permeate flow is of utmost importance. Nonlinear regression is used in this work to calculate parameters of two commonly used models from experimental data measured on a laboratory plant. During experiments, nanodiafiltration of solution containing lactose as macro-solute and sodium chloride as micro-solute was studied. A significant part of this work is dedicated to building an empirical model and estimation of its parameters. In comparison to traditional implicit or oversimplifying models, empirical model is proposed as a function of transmembrane pressure and macro-solute concentration. Subsequently, parameters of two distinct models are used for modelling and optimisation of a diafiltration process. Both empirical and traditional models are compared within a simulation and experimental data. In spite of higher water consumption during the diafiltration, the empirical model shows the preferable process operation in terms of the overall filtration time.

Keywords: diafiltration; fitting; modelling; nanofiltration; optimisation

Abstrakt

Optimalizácia diafiltračnej prevádzky akéhokoľvek membránového zariadenia z pohľadu dĺžky trvania procesu a spotreby rozpúšťadla zohráva dôležitú úlohu okrem iného aj v separačných procesoch potravinárskeho a farmaceutického priemyslu pri spracovávaní veľkých objemov suroviny. Okrem správneho odhadu základných parametrov filtračného systému je kľúčovým aspektom v zostavení matematického modelu filtračného procesu samotný model toku permeátu cez membránu. Na výpočet parametrov dvoch bežne používaných modelov je v tejto práci použitá nelineárna regresia z experimentálnych údajov nameraných na nanofiltračnej membránovej stanici pre vodný roztok laktózy ako makrozložky a chloridu sodného ako mikrozložky. Významnou súčasťou práce je zostavenie a určenie parametrov empirického modelu cezmembránového toku permeátu ako explicitnej funkcie cezmembránového tlaku a koncentrácie makrozložky na porovnanie s tradične používanými modelmi, ktoré bývajú buď implicitné alebo príliš zjednodušujúce. Parametre dvoch rôznych modelov sú následne použité na modelovanie a optimalizáciu diafiltračného procesu. Simuláciou a experimentálnym overením je vyhodnotená prípadová štúdia modelovania a optimalizácie, v ktorej sú porovnané dva modely toku permeátu—empirický a tradičný. Napriek väčšej spotrebe vody pri diafiltrácii sa ukázal empirický model ako výhodnejší z hľadiska celkového času filtrácie.

Kľúčové slová: diafiltrácia; fitovanie; modelovanie; nanofiltrácia; optimalizácia

Contents

Nomenclature

Symbol	*Meaning*
a	Coeficient in eqn. 5.6
A	Membrane area
b	Coeficient in eqn. 5.6
c	Coeficient in eqn. 5.6
c_i	Mass concentration of i-th solute
c_{lim}	Limiting concentration of macro-solute
C	Molar concentration
d	Coeficient in eqn. 5.6
e	Euler's number
j_0	Coeficient in eqn. 5.2
j_1	Coeficient in eqn. 5.2
J_j	Volumetric flux density of j-th stream
k	Mass transfer coefficient
M	Molar mass
n	Exponent in eqn. 3.9
p_1	Virial coeficient in eqn. 3.10
p_2	Virial coeficient in eqn. 3.10
p_3	Virial coeficient in eqn. 3.10
P	Hydrodynamic pressure
ΔP	Transmembrane pressure
q_j	Volumetric flux of j-th stream
R^2	Coefficient of statistical determination
R_i	Rejection coefficient of i-th solute
R_m	Membrane resistance in eqn. 3.8
R_M	Membrane resistance in eqn. 5.6
S	Singular arc
t	Time
T	Temperature
u	Pure solvent volumetric flux
V	System volume

Greek symbol	*Meaning*
α	Proportionality factor, eqn. 3.4
γ	Coefficient in eqn. 3.7
κ	Coefficient in eqn. 3.9
μ	Solvent viscosity
Π	Osmotic pressure
σ	Conductivity
Ψ	Electric potential
Subscript	*Meaning*
1	Macro-solute
2	Micro-solute
eff	Effective
f	Filtration
F	Feed
max	Maximum
P	Permeate
R	Retentate
w	Wall
Superscript	*Meaning*
*	Singular/switching
f	Final
init	Initial
Abbreviation	*Meaning*
C	Concentration
CVD	Constant-volume diafiltration
D	Dilution
GLF	Generalised limiting flux
LF	Limiting flux
MF	Microfiltration
NDF	Nanodiafiltration
NF	Nanofiltration
ODE	Ordinary differential equation
OP	Osmotic pressure
RMSE	Root-mean-square error
RO	Reverse osmosis
TMP	Transmembrane pressure
TR	Total recirculation
UF	Ultrafiltration
VVD	Variable-volume diafiltration

Chapter 1

Introduction

Membranes play a significant role in contemporary methods for separation processes owing to their favourable properties—effectiveness of separation, and lower costs and operation temperature compared to traditional (heat-assisted) processes. Thus, their use has become increasingly popular in (bio)chemical, pharmaceutical or food industry [2]. Furthermore, membranes found applications in promising electrical energy solutions, e.g. all-solid-state batteries or fuel cells [7].

Similarly to a biological membrane, a synthetic membrane may be defined as a barrier dividing two solutions with different concentrations of one or more *solutes* or suspended particles [12]. When an external impulse, for example hydrodynamic pressure of sufficient magnitude, is applied, forced mass transfer through the membrane occurs. The principle of separation is based on selective mass transfer of the components through the membrane. Components which pass through the membrane form a **permeate** stream, while those retained by the membrane form a **retentate** (or *concentrate*) stream.

In terms of streams configuration, there are two ways of introducing a feed stream to membrane:

- *cross-flow* filtration,
- *dead-end* filtration.

Both regimes are schematically shown in Fig. 1.1. In the former configuration, feed and retentate streams flow parallel to the membrane surface while permeate stream runs perpendicular, making it a preferred mode for continuous operations. In the latter configuration, however, no retentate stream is present. This implies continuously rising concentration on the feed side, leading even to formation of filtration cake, which causes gradual slowdown of the filtration resulting in completely ceased permeate flow [15].

Separation via membrane is based either on *sieve effect* or on *physico-chemical interactions* of separated component with membrane. In general, there are three types of driving force of the separation process [4]:

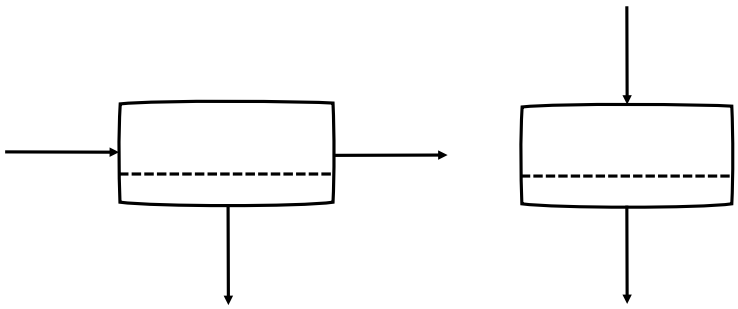

(a) Cross-flow regime (b) Dead-end regime

Figure 1.1: Two configurations of filtration

- *pressure* gradient – ΔP,
- *concentration* gradient – ΔC,
- *electric potential* gradient – $\Delta \Psi$.

Pressure-driven processes for separation in liquid phase are further divided into: *microfiltration* (MF), *ultrafiltration* (UF), *nanofiltration* (NF) and *reverse osmosis* (RO), depending on the *cut-off*[1] or electrostatic repulsion of particles by the membrane. Specific separation mechanism for common types of filtration system is exhaustively described in literature [12].

Membranes for *nanofiltration* (NF) (formerly referred to as *loose* or *low-pressure reverse osmosis*), characteristic for retention of divalent ions and organic (macromolecular) compounds, have found varied application especially in water and wastewater treatment, desalination [6], concentration of saccharide solutions, and other *non-aqueous* operations, namely *organic solvents recovery* [10].

Diafiltration is an operation or a sequence of operations using membrane filtration by which eventually one solute is concentrated and the other is diluted by clean solvent, which is usually the same as the one present in the solution prior to filtration. Three basic operation modes are thus possible [10]:

- *concentration* with at least one solute and one solvent,
- *purification* with at least two solutes and one solvent,
- *solvent exchange* with at least one solute and two solvents.

These modes are practically used, for example, in recoveries of valuable solvents,

[1] Cut-off is defined as the molecular weight of particles retained by a membrane for at least 90% [2].

desalination of macromolecular or protein solutions, or biochemical product separation [4]. Concentration-desalination principle is based on a selective membrane, which retains macro-solute, yet is permeable to solvent and micro-solute. The overall setup of diafiltration may be either batch or continuous.

In a batch membrane filtration system with *cross-flow* regime, three configurations are possible depending on presence of permeate recirculation: *no* recirculation (concentration or purification of the feed solution), *partial* recirculation or *total* recirculation (TR) of permeate to feed tank. TR configuration is used for steady-state measurements. Total or at least partial recirculation of retentate stream is necessary for filtration of batches of small volumes on either one, or on a small number of membrane filtration modules.

Processes on the industrial scale require maximum economic profitability, particularly by means of time efficiency and minimum feedstock consumption. Optimisation may be achieved via both suitable plant design by *chemical engineering* approach and favourable choice of dynamic degrees of freedom by *process control*. Over the last decades, information technology introduced so-called *optimising control* in order not only to regulate the industrial process but also to maintain its optimal conditions [15].

Chapter 2

Goal

Lactose is a disaccharide characteristic for its abundant presence in mammalian milk. Owing to its suitable properties, it has found numerous applications in pharmaceuticals mostly as an excipient[1], in baking as a crust browning agent or as a colour and flavour enhancing ingredient in protein containing products, and in dairy products for mimicking the human lactose content in cow's milk [8]. Industrial production of lactose is currently limited to whey processing, with nanodiafiltration (NDF) as one of feasible unit operations [20].

As mentioned in Chapter 1, the economic profitability of an industrial operation is often governed by process time and feedstock consumption. A goal of this work is to propose time-optimal conditions of a nanodiafiltration process. Furthermore, optimal strategy for water utilisation is also discussed.

In order to optimise the process, a mathematical model needs to be proposed. The most essential part of such model is specific term describing permeate flux. Subsequently, this work addresses a new model and compares it with standard models. In order to achieve this, model parameters of permeate flux for specific solvent-solute(s) system need to be determined. The estimation is based on experimental data fitting of permeate flux models given in section 3.3.3. The goodness of fit is to be evaluated and compared among the models.

The overall mathematical model of the process requires correct values of pertinent rejection coefficients and optimal control quantities for relevant flux models. Thus, these values need to be determined correctly in order to approach the real-system behaviour and the time-optimal strategy to the maximum achievable extent. The process and control quantities need firstly to be defined and calculated to obtain the complete time-optimal diafiltration strategy for the particular model of permeate flux.

Finally, the case study objective is to simulate optimal strategies for each model and to compare them with a non-optimal traditional one, applied in the context of the diafiltration process. Finally, the accuracy of calculated flux models is to be experimentally validated through case study measurements. Solvent-optimal strategies are discussed within the theoretical and simulation framework.

[1] a medicament carrier for tablets or inhalers

Chapter 3

Theoretical Background

3.1 Diafiltration Operation Modes

In diafiltration of one-solvent systems, one or more macro-solutes are concentrated and at least one micro-solute is washed out from the solution by addition of fresh solvent. Depending on volume change of batch system in question, four possible operation modes in relation to the macro-solute concentration may be considered [15]:

- **concentration** (C) mode – no solvent is added to the system, volume of the feed decreases,
- **constant-volume diafiltration** (CVD) mode – solvent is added to the system at the rate of permeate flow, the system volume is constant,
- **variable-volume diafiltration** (VVD) mode – flux of solvent to the system is lower than flux of permeate, the system volume decreases,
- **dilution** (D) mode – specific amount of pure solvent is added to the system in negligibly short period of time.

3.2 Fouling

Analogically to the cake formation in dead-end filtration regime, performance depression of filtration process can be observed also in cross-flow configuration. This trend is characterised by decreasing permeate flow in time, and often poses an unfavourable obstacle in continuous usage of membrane module. Fouling of membranes is described in literature [5, 14] in terms of causes, mechanism, modelling, and requisite measures to overcome this phenomenon. To maintain sufficient permeate flow, several solutions are considered, namely:

- *back-flow* of permeate,
- periodical *switching* to at least one fresh membrane module or
- *temperature* or *pressure adjusting profile* in time.

As fouling proved to have negligible effect on performance of the laboratory plant, it is not further considered in this work.

3.3 Mathematical Modelling of Diafiltration

A schematic diagram of a batch diafiltration process is shown in Fig. 3.1. The feed solution is pumped from the tank to the membrane module. Following selective separation on the membrane, the feed stream is divided to the retentate stream which continues in the recirculation to the feed tank, and to the permeate stream which is captured in another tank or disposed of. Steady-state mass balance of the membrane module for the two-solute system is given by the following equations

$$q_F = q_R + q_P, \tag{3.1a}$$

$$q_F c_{1,F} = q_R c_{1,R} + q_P c_{1,P}, \tag{3.1b}$$

$$q_F c_{2,F} = q_R c_{2,R} + q_P c_{2,P}, \tag{3.1c}$$

where q_j denote volume fluxes with respective concentrations $c_{i,j}$ for i-th solute and j-th stream, i.e. the feed ($j = F$), the retentate ($j = R$) and the permeate ($j = P$) streams.

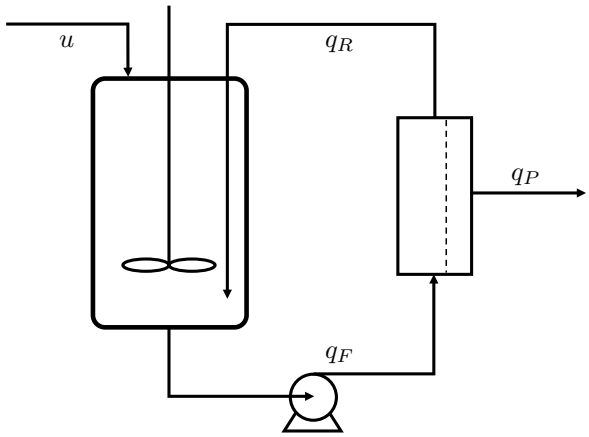

Figure 3.1: Scheme of diafiltration membrane separation unit

Overall volumetric permeate flux q_P is proportional to the membrane area

$$q_P = J_P A, \tag{3.2}$$

where J_P is the *permeate flux density* (or *velocity*, further referred to only as *permeate flux*) through the membrane of area A.

The driving force of the filtration process, *transmembrane pressure* (TMP) ΔP, is defined as a pressure drop on the membrane given by the equation

$$\Delta P = \frac{P_F - P_R}{2} - P_P. \tag{3.3}$$

Variables P_F, P_R and P_P designate hydrodynamic pressures in the feed, the retentate and the permeate streams respectively.

3.3.1 Proportionality Factor

An important diafiltration model variable—proportionality factor α—is defined as [15]

$$\alpha = \frac{u}{q_P}, \tag{3.4}$$

where u is flux of pure solvent to the feed tank.

Naturally, in C mode $\alpha = 0$, whereas in CVD mode $\alpha = 1$. If pure solvent flux is lower than permeate flux, then $\alpha < 1$ (VVD mode). The α value in D mode can be symbolically expressed as $\alpha = \infty$ [15].

3.3.2 Membrane Retention

Rate of retention of a substance by the membrane is expressed in terms of *rejection coefficient*, R, as

$$R_i = 1 - \frac{c_{i,P}}{c_{i,R}}, \tag{3.5}$$

where R_i is the rejection coefficient of i-th solute with concentrations $c_{i,P}$ and $c_{i,R}$ of permeate and retentate respectively.

For efficient separation of two solutes, the rejection coefficient of one solute should be approaching *unity* (macro-solute with negligible permeation through the membrane), while the other should be approaching *zero* (micro-solute with practically no retention by the membrane). In reality, rejection coefficients usually differ from *zero* or *unity*, which is discussed in subsequent chapters.

3.3.3 Permeate Flux Model

The most essential part of membrane process modelling is a model of transmembrane mass transfer or the *permeate flux model*. There are generally two ways to describe such transport mechanism. The first one considers the membrane as a *black box* and is based on irreversible thermodynamic principles such as Gibbs energy dissipation and entropy production [10]. The second approach requires deeper understanding of the membrane transport phenomena based on the membrane structure [10]. Within this more fundamental (mechanistic) method, there are two basic structural concepts of the membrane:

- a *dense* membrane described by a *solution-diffusion* model,
- a *porous* membrane described by a *pore-flow* model.

The former considers solute-solvent-membrane behaviour, while the latter is highly friction-based. All three kinds of models are described in literature together with semi-empirical and combined models accounting for imperfection corrections [10].

3.3.3.1 Limiting Flux Model

In ultrafiltration (UF) of solutions containing proteins or substances with tendency to form a gel layer on membrane with no macro-solute present in the permeate, the *gel layer* or *limiting flux model* was proposed [3]

$$J_P(c_1) = k \ln \frac{c_{lim}}{c_1}, \tag{3.6}$$

where k is mass transfer coefficient of macro-solute in the laminar film on membrane, c_{lim} is 'limiting' concentration (also denoted c_g referring to 'gel' concentration) on membrane and c_1 is bulk concentration of macro-solute on the feed/retentate side of membrane.

Eqn. 3.6 can be derived from the *film theory* by integration of the mass balance equation of solute flux on membrane. It was shown that this model can be reliably used also for modelling of NF, even though the parameter c_{lim} is only phenomenological with no deeper physical meaning [9]. While reaching the limiting concentration of the macro-solute on the membrane, the model suggests no significant pressure-affected flux change, hence the name 'limiting'. For simplicity, this model assumes parameters k and c_{lim} to be constant at given TMP and temperature. This, however, poses a drawback when pressure or viscosity effects need to be taken into account.

3.3.3.2 Generalised Limiting Flux Model

As indicated in eqn. 3.6, the LF model is a function of the macro-solute concentration only. In the work [17], a specific type of LF model was proposed

$$J_P(c_1, c_2) = k \ln \frac{c_{lim}}{c_1 c_2^{\gamma}}, \tag{3.7}$$

with the micro-solute concentration c_2 (uniform in the whole system if $R_2 = 0$) and an additional coefficient γ. This model, termed in [19] as the *generalised limiting flux* (GLF) model, includes the influence of the micro-solute on permeate flux.

3.3.3.3 Osmotic Pressure Model

One of the most universal and most popular models for modelling of the permeate flux is the *osmotic pressure model*. This model is derived from the solution-diffusion approach and can be used practically for any type of pressure-driven membrane filtration. The form of the model equation is following

$$J_P(c_1) = \frac{\Delta P - \Delta \Pi(c_1)}{\mu R_m}, \tag{3.8}$$

where $\Delta \Pi(c_1)$ is osmotic pressure caused by the gradient of concentration of the macro-solute on both membrane sides, μ is the solvent viscosity, and R_m is the temperature- and solute-independent membrane resistance.

Based on van't Hoff's equation and the film theory, osmotic pressure on membrane can be according to [21] expressed as

$$\Delta \Pi = \kappa c_1^n \exp \frac{n J_P}{k}, \tag{3.9}$$

where κ is a constant and n is an exponent equal approximately to *two* for macromolecular solutions. Osmotic pressure can also be rewritten in the form of virial equation

$$\Delta \Pi = p_1 c_{1,w} + p_2 c_{1,w}^2 + p_3 c_{1,w}^3, \tag{3.10}$$

where p_1, p_2 and p_3 are parameters of corresponding virial equation and $c_{1,w}$ is flux-dependent macro-solute wall concentration. Osmotic pressure (OP) model is therefore implicit, assumes unlimited rise of permeate flux with increasing transmembrane pressure and often fails in description of NF [10]. Under simplifying assumptions

in [21], following explicit form was derived

$$J_P(c_1) = \frac{k}{n} \ln \frac{\Delta P}{\kappa c_1^n}, \tag{3.11}$$

which is equivalent to the LF model 3.6 if $c_{lim} = \sqrt[n]{\frac{\Delta P}{\kappa}}$.

3.3.3.4 Empirical Model

In the work [18], three empirical models for modelling of UF whey separation were presented. Assuming negligible fouling, the following model can be obtained using the *exponential empirical resistance*

$$J_P(c_1, \Delta P) = J_{P,max}(c_1) \left(1 - \exp \frac{-\Delta P}{R_M}\right), \tag{3.12}$$

with pressure-indepentent maximum flux $J_{P,max}(c_1)$ as a function of macro-solute bulk concentration and R_M as a membrane resistance constant. This model is to be adapted and discussed later in this work.

3.4 Process Model

Assuming a system containing three components: a solvent, a macro-solute and a micro-solute; with the configuration of the process shown in Fig. 3.1, mass balance of the system volume and solutes can be expressed as a set of following differential equations [15]

$$\frac{\mathrm{d}c_1}{\mathrm{d}t} = \frac{c_1 q_P}{V}(R_1 - \alpha), \quad c_1(t=0) = c_1^{init}, \tag{3.13a}$$

$$\frac{\mathrm{d}c_2}{\mathrm{d}t} = \frac{c_2 q_P}{V}(R_2 - \alpha), \quad c_2(t=0) = c_2^{init}, \tag{3.13b}$$

$$\frac{\mathrm{d}V}{\mathrm{d}t} = (\alpha - 1) q_p, \qquad V(t=0) = V^{init}, \tag{3.13c}$$

where V is the volume of the system, c_i and R_i are concentrations and rejection coefficients of both the macro-solute ($i = 1$) and the micro-solute ($i = 2$). These concentrations are practically identical for the feed and the retentate streams if $q_R \gg q_P$, as can be shown from mass balance equations 3.1.

3.5 Process Optimisation

Diafiltration process is often conducted in batches, where two major factors are of economic concern: *minimum fresh solvent consumption* and *minimum time of the overall process*.

In [15], time-optimal strategy for diafiltration process is derived. It suggests a three-step optimal approach consisting of different operational modes described in Section 3.1. Generally, following strategy is optimal:

1. Macro-solute is concentrated to *switching* (*singular*) concentration c_1^* – C mode.
2. Micro-solute is washed-out from the feed solution to obtain required ratio of solutes concentrations – CVD or VVD mode depending on α.
3. If $c_1^f < c_1^*$ (c_1^f denotes the desired final concentration of the macro-solute), the solution is instantaneously diluted by specific amount of pure diluent (solvent) to obtain required final concentrations c_1^f and c_2^f – D mode.

The singular conditions, i.e. the switching concentration of the macro-solute and the α ratio during the purification, are given for the time-optimal control according to [19] by conditions

$$S = q_P + \frac{\partial q_P}{\partial c_1} c_1 + \frac{\partial q_P}{\partial c_2} c_2 = 0, \tag{3.14}$$

$$\alpha = \frac{\frac{\partial S}{\partial c_1} c_1}{\frac{\partial S}{\partial c_1} c_1 + \frac{\partial S}{\partial c_2} c_2}, \tag{3.15}$$

where S denotes a singular/sensitivity arc from a non-linear feedback control described in [15].

For the limiting flux model 3.6, the optimal conditions are then

$$S = q_P - k = 0, \qquad \text{if} \qquad c_1^* = \frac{c_{lim}}{e}, \tag{3.16}$$

$$\alpha = 1, \tag{3.17}$$

since in accordance with equations 3.2 and 3.6, the permeate flux is a function of the macro-solute concentration only. On the other hand, application of the optimal

conditions 3.14 and 3.15 on the generalised limiting flux model yields

$$S = q_P - k(\gamma + 1) = 0, \qquad \text{if} \qquad c_1^*(c_2) = \frac{c_{lim}}{e^{\gamma+1} c_2^{\gamma}}, \tag{3.18}$$

$$\alpha = \frac{1}{1+\gamma}, \tag{3.19}$$

where the switching $c_1^*(c_2)$ is a function of the micro-solute and $\alpha < 1$ assuming $\gamma > 0$, which is in line with the prediction made by the VVD mode in the second diafiltration step described on page 5.

In addition, the solvent-consumption optimal strategy shifts the switching to the limiting concentration of the macro-solute, $c_1^* = c_{lim}$ for the LF model in accordance with [16]. However, this approach is practically limited by the actual (macro-solute) solubility in the solvent. The switching concentration, c_1^*, can therefore not exceed the value of this solubility, since undesirable crystallisation may occur. Moreover, at high solute concentrations, the permeate flux drops to very low rates, resulting in excessively long periods of filtration, which makes the minimum-solvent strategy consideration impractical.

Optimal control problem for the empirical model in the form of eqn. 5.6 requires, as discussed later, a numerical solution, since no analytical form of the switching concentration, c_1^*, can be expressed from the condition 3.14. The mode of diafiltration during the washing mode, i.e. the α ratio for this model, is CVD ($\alpha = 1$), as long as the empirical model is a function of the macro-solute concentration only. Similarly to the previous case, the switching concentration for the solvent-consumption-minimising strategy is for the empirical model constrained also by the macro-solute solubility. In Chapter 5, this limitation is even augmented by the value of one of the model coefficients, for which the permeate flux is limited to *zero*.

Chapter 4

Methodology

In this work, water solutions containing various concentrations of lactose (macro-solute) and sodium chloride (micro-solute) were subjected to experimental nanodiafiltration (NDF) measurements. Several data series were obtained for the model parameters estimation using these chemicals:

- lactose monohydrate (99.9 %, $M = 360.31\,\mathrm{g/mol}$, Centralchem, s.r.o., Slovakia),
- sodium chloride (99.9 %, $M = 58.44\,\mathrm{g/mol}$, Centralchem, s.r.o., Slovakia),
- reverse-osmosis water ($\sigma \in [7, 20]\,\mu\mathrm{S/cm}$).

The scheme of the laboratory plant used for membrane filtration is in Fig. 4.1. The feed stream was pumped through a spiral-wound nanofiltration module NFW (cut-off range 300-500 Da, membrane area $A = 0.465\,\mathrm{m}^2$, $\Delta P_{max} = 30\,\mathrm{bar}$, Synder Filtration, USA) in TR mode of the retentate. Transmembrane pressure (TMP) was regulated by a pressure controller (PC) and an actuator HANBAY (V1) after the membrane module. Pressures of both permeate and retentate streams were measured by two WIKA A-10 pressure transmitters (PT1 and PT2) with pressure range from 0 to 1000 bar. Volume fluxes were measured by BIOTECH VZS-005-VA (FT2 for the *permeate*, flow range 0.005 to 1.75 L/min), and Greisinger Vision 2008/1 (FT1 for the *retentate*, flow range 0.5 to 25 L/min), the feed tank volume was measured by a level transmitter (LT) WIKA S-11. Temperatures and conductivities were recorded by Mettler Toledo, easySense Cand 73 (TT2 and AT2 for the *permeate*, measuring range 0.1 to 2000 µS/cm) and easySense Cand 77 (TT1 and AT1 for the *retentate*, measuring range 0.02 to 400 mS/cm). The retentate stream was cooled by a plate and frame heat exchanger, with the system temperature regulated in the range $T \in [21.5, 22.5]\,^{\circ}\mathrm{C}$ by a temperature controller (TC) and an actuator (V2) during all performed experiments.

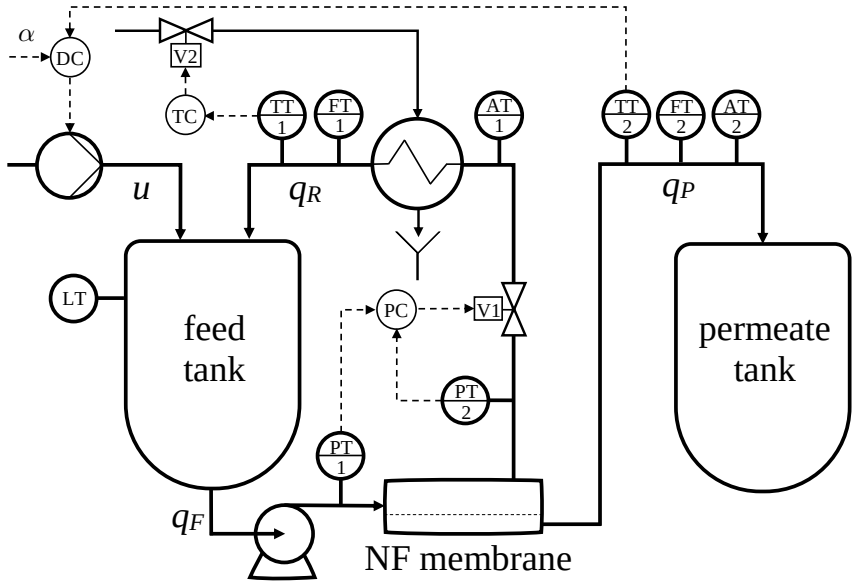

Figure 4.1: Simplified P&ID scheme of the nanofiltration laboratory plant

4.1 System Parameters Calculation

4.1.1 NaCl Concentration Calibration Curve

The linear concentration-conductivity function from [19] was experimentally verified on a benchtop EC meter HI5522-01 (Hanna Instruments, Inc., USA):

$$\frac{c_2}{\mathrm{g/L}} = 0.0007 \cdot \frac{\sigma}{\mathrm{\mu S/cm}} - 0.6949. \tag{4.1}$$

This equation was used further for all sodium chloride concentration measurements.

4.1.2 Piping Volume

The volume of feed in the tank in Fig. 4.1 was measured in the range from 3.50 L to 35.00 L (maximum capacity of the feed tank) with error of ±0.02 L. Neglecting the piping volume would lead to significantly inaccurate computed values of the lactose concentration, especially for the lower tank-volume region. For more accurate lactose concentration estimations, the whole system volume needed to be quantified. In five measurements, specific amount of NaCl was added to the system. The overall system volume was computed as the product of amount of NaCl and given concentration (calculated from measured conductivity using the calibration curve 4.1). The piping

volume was the difference between the tank volume and the overall system volume. The average piping volume value was thus established to be 3.00 L.

4.2 Data Collection

The osmotic pressure (OP) model as defined by eqn. 3.8 predicts linear flux-TMP dependency. This was verified by measuring permeate fluxes at various TMP values in the range of $\Delta P \in [0, 25]$ bar for pure water. At different TMP set points, permeate fluxes were measured in the total recirculation (TR) mode, as described in Chapter 1. An example of such measurement is shown in Fig. 4.2. According to eqn. 3.2, steady-state values of permeate fluxes were averaged and divided by the membrane area. In subsequent calculations, values of these permeate fluxes (more precisely *flux densities*) were taken into account.

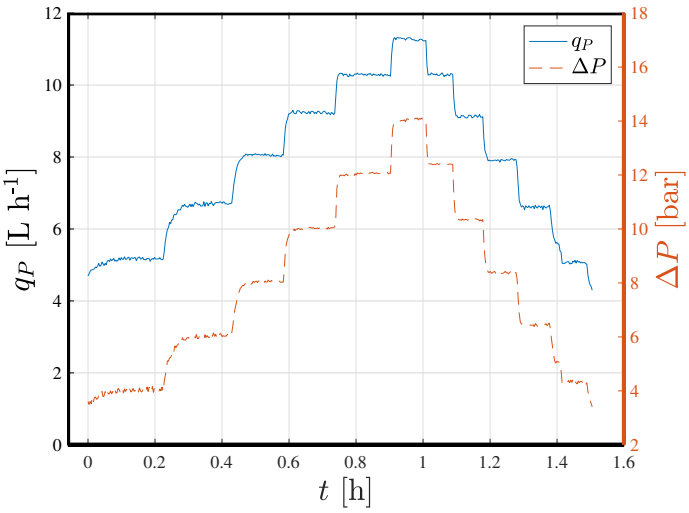

Figure 4.2: Example of measurement of q_P at different ΔP in time

For solutions containing various concentrations of lactose and sodium chloride, measurements of the permeate flux at different TMPs were performed, similarly to the measurement with pure water. Altogether, twenty-one different measurement were conducted for concentration region shown in Fig. 4.3. Aside from pure NaCl or pure lactose solutions, six distinct $[c_1, c_2]$ combinations (yellow circles in Fig. 4.3) were distributed by *latin hypercube sampling* [11] calculated by a dedicated MATLAB function. The overall variable domain regarding TMP values is depicted by a 3D-graph in Fig. 4.4. These data series were also measured in the TR mode.

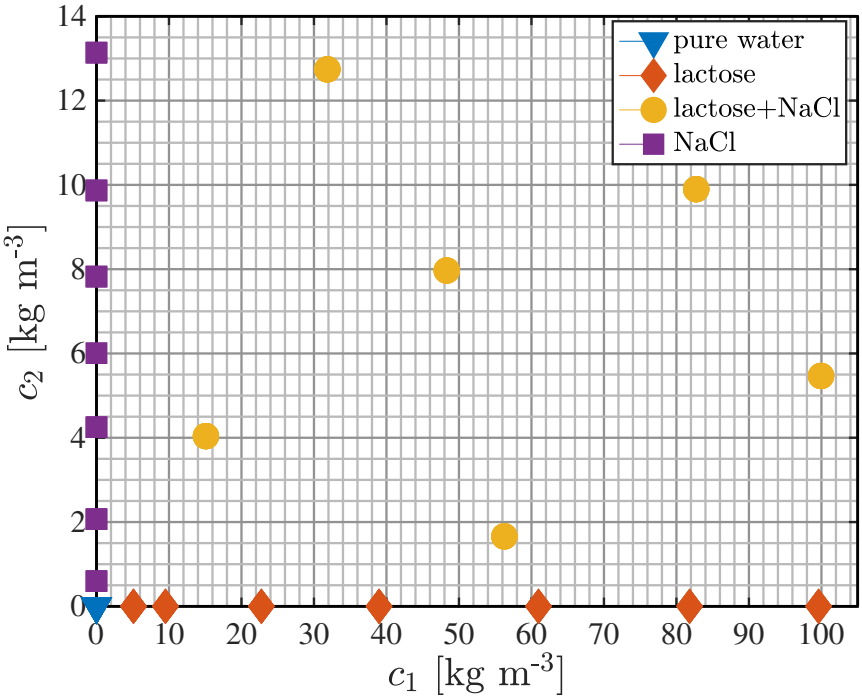

Figure 4.3: The domain of concentrations c_1 and c_2

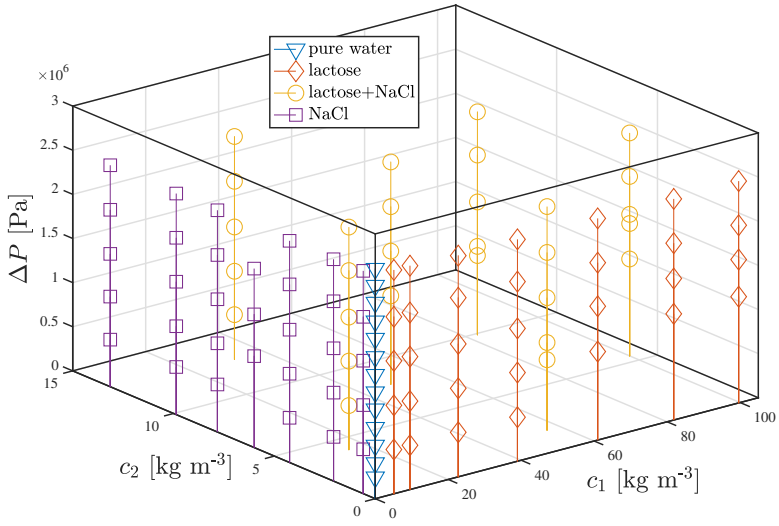

Figure 4.4: The domain of variables

In this work, all computations were performed using MATLAB 2017b. Model parameters for three permeate flux models were firstly calculated using non-linear least-squares data fitting functions in Optimization Toolbox. The resulting data fitting and statistical evaluations were performed via the '`fit`' function in MATLAB. For dynamic regression and for case study simulations, '`ode15s`' and '`ode45`' solvers were utilised.

4.3 Parameters Estimations

While equations 3.6 and 3.7 were directly utilised in regression to obtain the isobaric model parameters for both LF and GLF models at $\Delta P = 20.2\,\text{bar}$, the empirical model was implemented to model the $J_P(c_1, \Delta P)$ behaviour. Equation 3.12 was the starting point to find a new explicit form of such model. The analysis for proposal of the specific form is illustrated in Fig. 4.5.

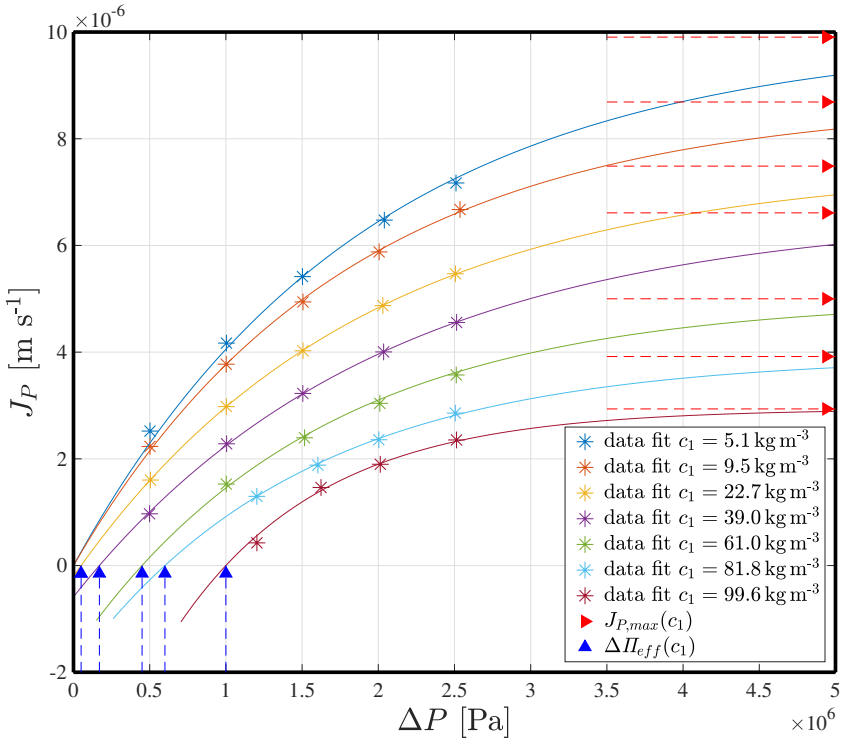

Figure 4.5: Initial fitting of function $J_P(c_1)$

As seen from initially fitted isoconcentration dependencies at higher lactose concentrations, the permeate flux does not equal *zero* as predicted by eqn. 3.12. Therefore,

a modification of the equation was made to the form

$$J_P(c_1, \Delta P) = J_{P,max}(c_1) \left(1 - \exp \frac{\Delta \Pi_{\text{eff}}(c_1) - \Delta P}{R_M}\right), \tag{4.2}$$

with an additional parameter of the 'effective' osmotic pressure, $\Delta \Pi_{\text{eff}}(c_1)$, which could be described as the osmotic pressure at bulk concentration c_1 or the TMP at which the permeate flux is equal to *zero*.

Secondly, each isoconcentration series yielded respective values of parameters of the maximum permeate flux (velocity), $J_{P,max}(c_1)$, the 'effective' osmotic pressure $\Delta \Pi_{\text{eff}}(c_1)$ and the membrane resistance R_M. Subsequently, suitable forms of lactose-concentration functions of the first two parameters were chosen, which is described further in Section 5.3.

4.4 Rejection Coefficients

The membrane solute-separation characteristics—rejection coefficients introduced in 3.3.2—were also estimated to achieve highest possible fidelity of case study simulations. While the lactose rejection coefficient was assumed $R_1 = 1$[1] for simplicity, the NaCl rejection was estimated by Dynamic Optimisation and static calculation from three different measurements.

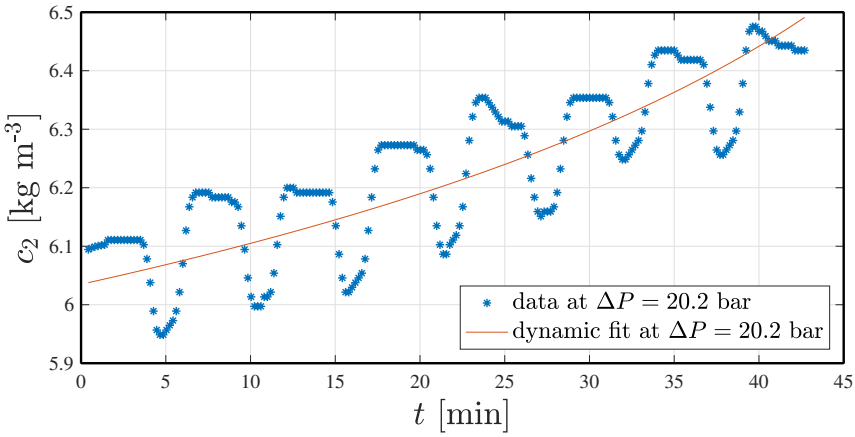

Figure 4.6: Dynamic fitting of the salt rejection coefficient, R_2

[1] Minimum rejection of lactose declared by the membrane manufacturer is $R_1 = 0.985$ at $c_1 = 2\,\text{g/L}$, $\Delta P = 7.60\,\text{bar}$ and $T = 25\,^\circ\text{C}$.

In the dynamic estimation, the rising sodium chloride concentration in time was fitted via minimising the difference between the values measured in time and the values integrated by the model ODEs 3.13. The modified parameter for finding the minimum of the objective function was the rejection coefficient, R_2. Graphical illustration of the dynamic fitting is depicted in Fig. 4.6 (oscillations of the concentration values were caused by imperfect temperature regulation mentioned in the beginning of this Chapter).

For static R_2 estimations, equation (9.30) in [4], derived from the rejection coefficient definition 3.5 and the batch system micro-solute differential mass balance, was rearranged to

$$R_2 = \frac{\ln \frac{c_2^f}{c_2^{init}}}{\ln \frac{V^{init}}{V^f}}, \tag{4.3}$$

where c_2^{init} and c_2^f are steady-state salt concentrations in the TR mode before and after the filtration mode with no permeate recirculation, and V^{init} and V^f are respective system volumes. This approach is illustrated in Fig. 4.7 for a measurement containing lactose at $\Delta P = 23.6\,\text{bar}$.

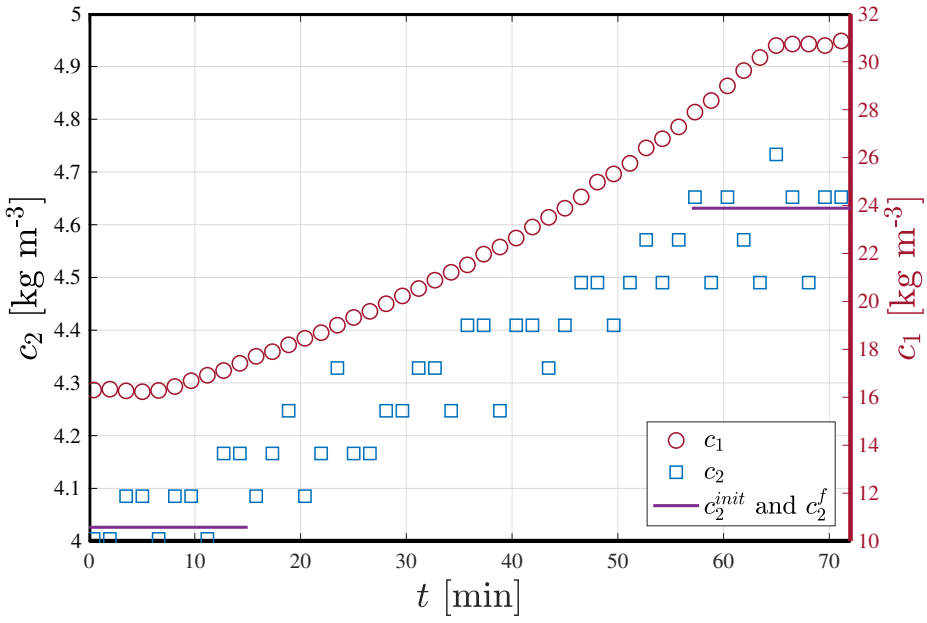

Figure 4.7: Static estimation of R_2 with lactose present

Chapter 5

Results and Discussion

5.1 Osmotic Pressure Model – Pure Solvent Flux

According to eqn. 3.8, linearity of the osmotic pressure model was examined as mentioned in 4.2. Steady-state permeate fluxes were plotted against respective averaged TMP values. Various authors, for example in [1], use this approach to plot a linear dependency

$$J_P = \frac{\Delta P}{\mu R_m}, \tag{5.1}$$

with a slope $\frac{1}{\mu R_m}$ and membrane resistance, R_m, being a constant accordingly. In Fig. 5.1, the measured data do not follow such dependency and tend to form a curve instead of a straight line, indicating non-linear (*limiting flux*) dependency. Use of the R_m value from linear function 5.1 for further experimental calculations with $\Delta\Pi > 0$ would be inadequate and might lead to major errors. Although observation of *limiting* flux has frequently been reported [21], for pure solvent, this issue has been dealt by fewer authors [18].

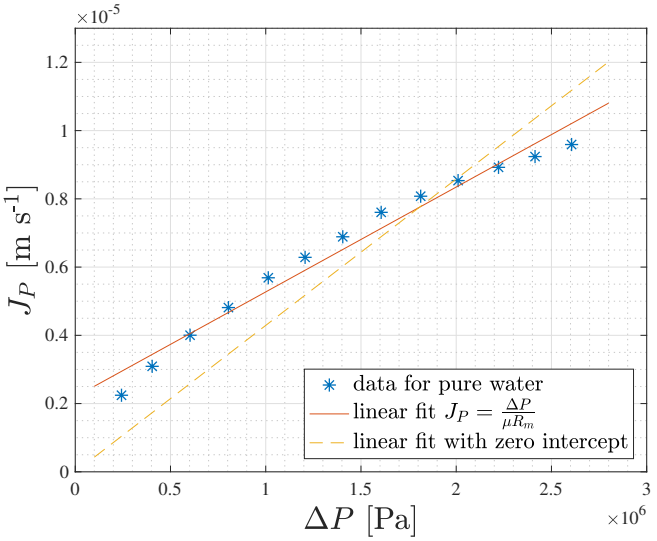

Figure 5.1: Limiting permeate flux of pure solvent (water) versus TMP

5.2 Limiting Flux Models Fitting

Similarly to measurements with pure water, permeate fluxes of solute(s)-containing solutions were recorded. Measurements in the domain shown in Fig. 4.4 gave the value range of fluxes depicted in Fig. 5.2.

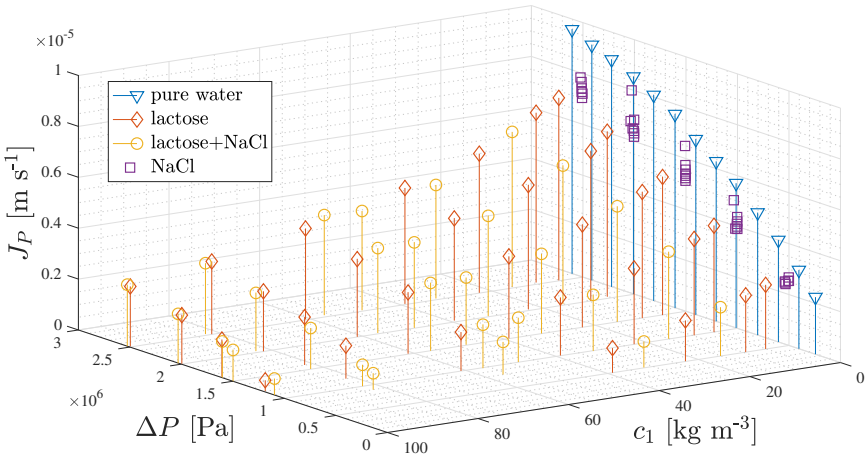

Figure 5.2: Permeate fluxes versus lactose concentration and TMP

To fit the GLF model 3.7, data series at a specific TMP value was used to estimate the isobaric model parameters, as mentioned in 4.3. For these fits, only the data with $c_1 > 0$ was used[1]. Fits for two different TMP data series are shown in Fig. 5.3. Parameters at $\Delta P = 20.2\,\text{bar}$ are listed in Table 5.1. It can be seen that along the given range of NaCl concentrations, the flux is practically invariant for both surfaces representing fits at two TMPs. Moreover, the γ value in Table 5.1 falls within a 95% confidence interval crossing *zero*, thus considering the c_2 influence is redundant and the GLF model unnecessary for modelling.

Table 5.1: Fitted model parameters for GLF and LF models at $\Delta P = 20.2\,\text{bar}$

model	**GLF**	**LF**
k [m s^{-1}]	$(1.602 \pm 0.193) \times 10^{-6}$	$(1.600 \pm 0.176) \times 10^{-6}$
c_{lim} [kg m^{-3}]	384.6 ± 113.0	384.4 ± 106.2
γ [1]	$(-5.2 \pm 163.9) \times 10^{-4}$	–
R^2	0.9732	0.9732
RMSE	2.728×10^{-7}	2.602×10^{-7}

[1]For numerical reasons, values of $c_2 = 0$ in data series were substituted with the value of $10^{-5}\,\text{kg/m}^3$ in the GLF model 3.7 fitting.

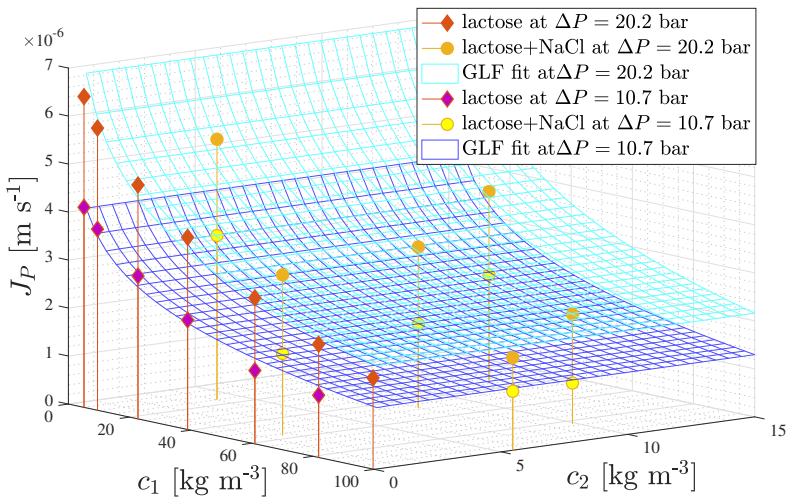

Figure 5.3: Fits of the GLF model at two different TMPs

As for the GLF fitting, the same data was used to obtain the LF model. The fits were plotted in Fig. 5.4, each line indicating one fit at given TMP value. The model parameters, fitted for this model at $\Delta P = 20.2$ bar, are also listed in Table 5.1. Root-mean-square errors (RMSE) for each of the both models are similar and coefficients of determination (R^2) achieve identical values, therefore use of the LF model instead of the GLF model for further modelling is viable. Confidence interval of c_{lim} suggests a significant difference between subsequent modelling and experimental verification.

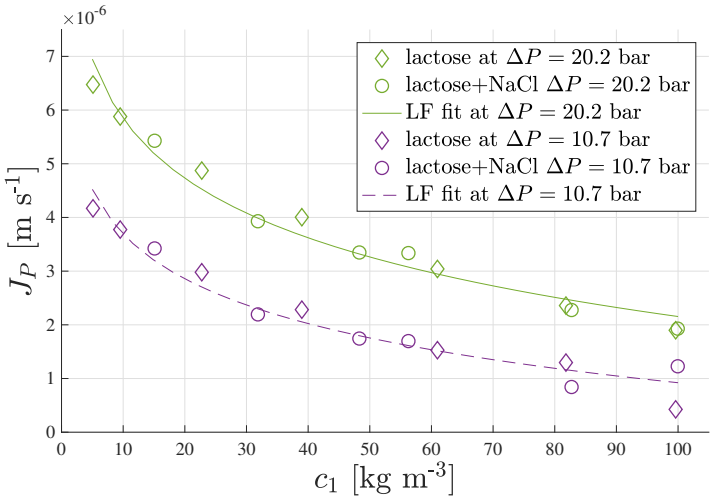

Figure 5.4: Fits of the LF model at two different TMPs

5.3 Empirical Model Fitting

As introduced in the previous chapter, empirical model function 4.2 was proposed to examine direct pressure-dependency of the permeate flux. Thus, pure water and isoconcentration (regarding lactose only) data series were subjected to further analysis, so as to propose a complete form of the model.

5.3.1 Maximum Permeate Flux

In both the LF and GLF model, the limitation of flux at constant pressure is given by rising concentration of macro-solute. The permeate flux, therefore, reaches the limit of *zero* either when the mass transfer coefficient k approaches *zero* or when c_1 is close to c_{lim}[2]. On the other hand, the maximum permeate flux, $J_{P,max}(c_1)$, in the $J_P(c_1, \Delta P)$ dependency is solely a function of lactose concentration, as can be seen in Fig. 4.5.

In order to find the specific function $J_{P,max}(c_1)$, fitted values of $J_{P,max}$ (red right-pointing arrows in Fig. 4.5) for corresponding concentrations of lactose were plotted against the c_1 values to obtain the plot in Fig. 5.5. The form of the $J_{P,max}(c_1)$ function was also proposed as [18]

$$J_{P,max}(c_1) = \frac{1}{j_0 + j_1 c_1}, \tag{5.2}$$

where j_0 and j_1 are constant coefficients. This function, however, does not provide a satisfactory fit for the data measured in this work, as shown in Fig. 5.5. Therefore, an implicit function was suggested in the form of a quadratic equation

$$c_1 = a J_{P,max}^2 + b J_{P,max} + c, \tag{5.3}$$

with pressure- and concentration-independet coefficients a, b and c, which can be rearranged into an explicit form

$$J_{P,max} = \frac{-b - \sqrt{b^2 - 4a(c - c_1)}}{2a}. \tag{5.4}$$

Only subtraction of the discriminant square root in the numerator gives a physically-meaningful result. Values of coefficients obtained in this fashion are listed in Table 5.2. Interestingly, the parameter c, corresponding to concentration which when attained

[2]Without simplifications accepted in 3.3.3.1, both $k(c_1)$ and $c_{lim}(c_1)$ parameters are dependent also on c_1, hence they vary with rising c_1.

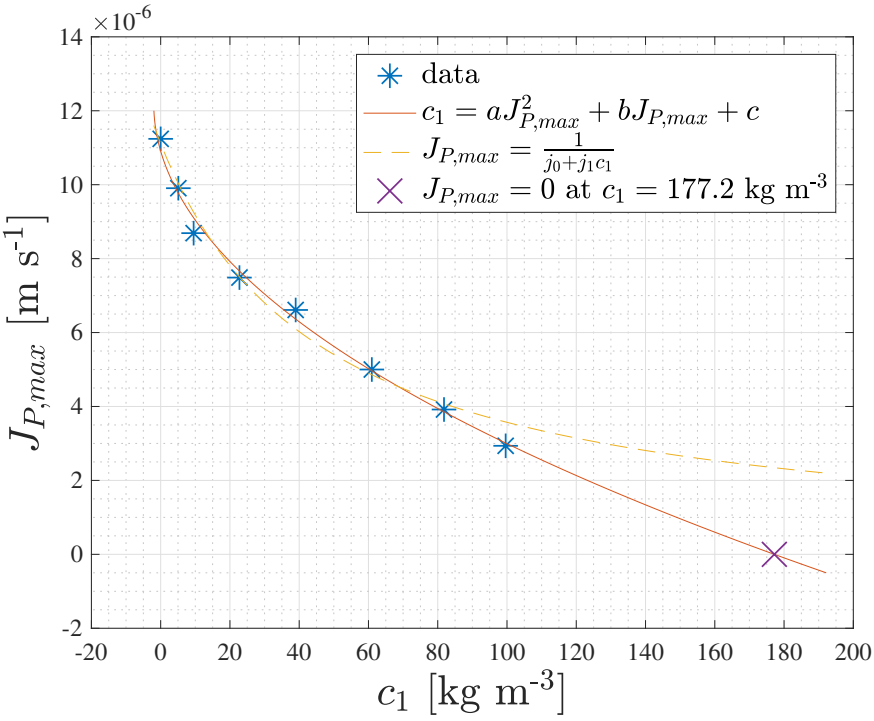

Figure 5.5: Fitting of function $J_{P,max}(c_1)$

(violet cross in Fig. 5.5) results in $J_{P,max} = 0$, is approximately equal to lactose solubility[3].

Table 5.2: Fitted coefficients for the parameter $J_{P,lim}(c_1)$ of the empirical model

a [kg s^2 m^{-1}]	$(1.205 \pm 0.357) \times 10^{12}$
b [kg s m^{-2}]	$(-2.938 \pm 0.509) \times 10^{7}$
c [kg m^{-3}]	177.2 ± 16.2
R^2	0.9935
RMSE	2.2067×10^{-7}

5.3.2 Pressure at Zero Permeate Flux

Analogically, *effective* osmotic pressure values (blue upward-pointing arrows in Fig. 4.5) versus lactose concentrations were plotted in Fig. 5.6. A simple fitting function was proposed

$$\Delta\Pi_{\text{eff}}(c_1) = d\, c_1^2, \tag{5.5}$$

[3] 170.3 g/L at 22 °C according to [13]

where $d = (99.6 \pm 7.5)\,\mathrm{Pa\,m^6\,kg^{-2}}$ is a coefficient also independent on pressure and concentration.

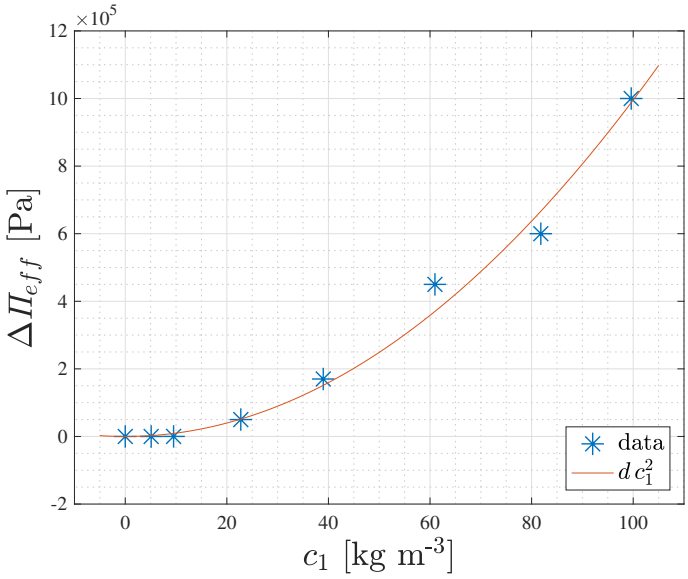

Figure 5.6: Fitting of function $\Delta\Pi_{\mathrm{eff}}(c_1)$

5.3.3 Membrane Resistance

Finally, the third parameter of the empirical model 4.2 was estimated. Its value for each fitted series in Fig. 4.5 was plotted in Fig. 5.7 versus the pertinent concentration. This parameter may be considered constant for a given membrane, with its average value for the fitting evaluated to be $R_M = 1.638 \times 10^6\,\mathrm{Pa}$.

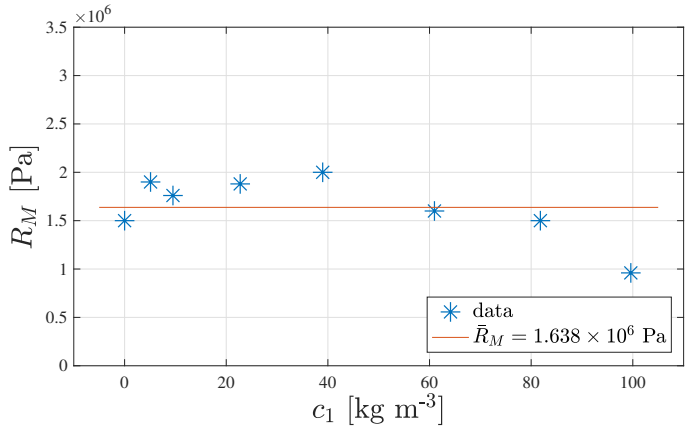

Figure 5.7: Membrane resistance R_M versus lactose concentration c_1

5.3.4 Fitting of the Whole Model

The parameters fitted in the previous three sections were used as an estimate values for the overall empirical parameters estimation. Fitted values of this estimation are listed in Table 5.3. The data series used for fitting were the same as in 5.2. Combining equations 4.2,5.4 and 5.5, the final complete form of the empirical model was obtained

$$J_P(c_1, \Delta P) = \frac{-b - \sqrt{b^2 - 4a(c - c_1)}}{2a} \left(1 - \exp \frac{dc_1^2 - \Delta P}{R_M}\right). \tag{5.6}$$

The surface of this function with the fitted parameters can be found in Fig. 5.8 (to be compared with Fig. 5.2).

Table 5.3: Fitted coefficients for empirical model

ΔP [bar]	[0.5, 25.2]	20.2
a [kg s^2 m^{-1}]	$(2.00 \pm 1.31) \times 10^{12}$	$(0.91 \pm 216.10) \times 10^{12}$
b [kg s m^{-2}]	$(-3.75 \pm 1.39) \times 10^{7}$	$(-2.52 \pm 297.9) \times 10^{7}$
c [kg m^{-3}]	(170.5 ± 34.3)	(167.9 ± 985.3)
d [Pa m^6 kg^{-2}]	(74.4 ± 33.0)	(19.9 ± 2703.0)
R_M [Pa]	$(1.00 \pm 0.21) \times 10^{6}$	$(2.15 \pm 419.25) \times 10^{6}$
R^2	0.9466	0.9818
RMSE	3.9430×10^{-7}	2.5134×10^{-7}

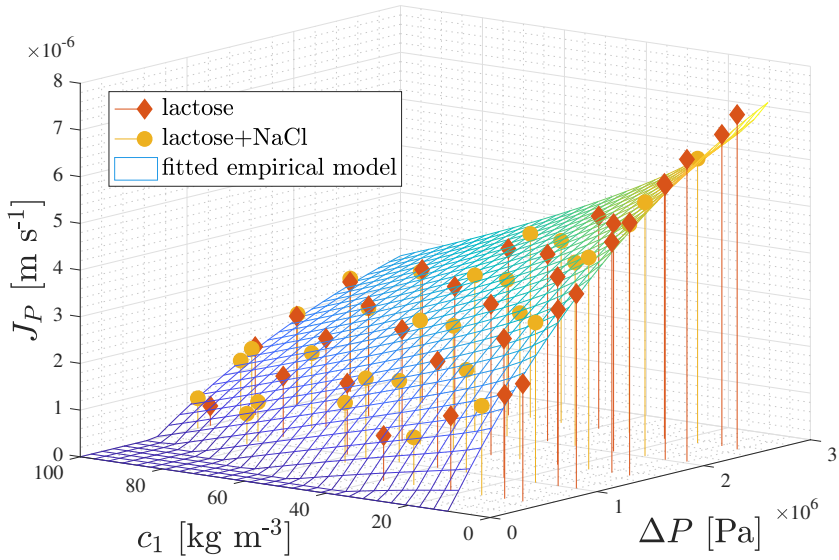

Figure 5.8: Fitted empirical model compared with measured data

Fitting at fixed $\Delta P = 20.2\,\text{bar}$ was also performed and resulting coefficients listed in Table 5.3 were used for the case study simulation. Similarly to c_{lim} in Tab. 5.1, these values fall within a wide confidence interval, indicating a small size of data sample relative to the number of fitted parameters. Comparison of LF and empirical models fits at $\Delta P = 20.2\,\text{bar}$ is illustrated in Fig. 5.9. Note that unlike by the former one, permeate flux by the latter model drops to *zero* at $c_1 = 167.9\,\text{kg m}^{-3}$, which is the value of c coefficient in Tab. 5.3. This is considered in the subsequent optimisation with respect to water consumption.

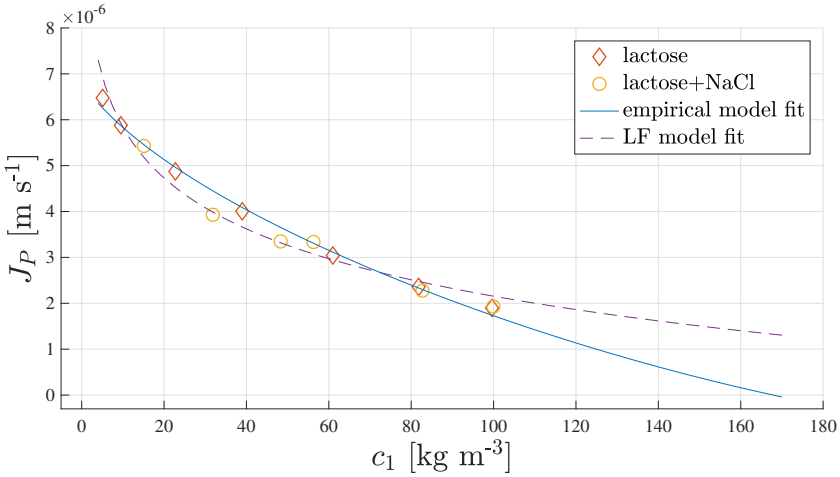

Figure 5.9: Fitted empirical and LF models at $\Delta P = 20.2\,\text{bar}$

5.4 NaCl Rejection Coefficient Estimation

As discussed in Section 4.4, the lactose rejection coefficient, R_1, was assumed to be equal to *unity*, while the sodium chloride rejection coefficient, R_2, was assumed to be a constant greater than *zero* and was experimentally determined.

For solutions containing no lactose ($c_1 = 0$), R_2 was estimated using both Dynamic Optimisation and static computation, as shown in Fig. 4.6 and 4.7 respectively. In the solution with non-zero concentration of lactose, the rejection coefficient was estimated using static approach. Altogether, all values of R_2 are presented in Table 5.4.

Although this data corresponded to the data provided by the membrane manufacturer[4] for solutions containing no lactose, the rejection coefficient of sodium chloride for case

[4] $\bar{R}_2 = 0.200$ at $c_2 = 2\,\text{g/L}$, $\Delta P = 7.60\,\text{bar}$ and $T = 25\,^\circ\text{C}$

study simulations was eventually assumed $R_2 = 0$. Note, that the rejection coefficient in lactose solution (row 3 in Tab. 5.4) achieves only around 80% of the R_2 value, when no lactose is present. When lactose concentration more than twice as high was used, an unexpected phenomenon of the negative rejection was observed in case study measurements, as discussed in the next Section. To demonstrate the deviation of the reality from simulation results caused by this phenomenon, the value of R_2 was further considered *zero* (i.e. no retention of the salt by the membrane), as typically assumed by various authors for simplification [15].

Table 5.4: Calculated values of constant rejection coefficient, R_2

c_1 [kg m^{-3}]	R_2	approach
0	0.2022	dynamic
0	0.2046	static
[16.3, 30.7]	0.1663	static

5.5 Simulations and Experimental Operation

Having estimated coefficients of the LF model, optimality parameters for this model were evaluated using equations 3.16. For the empirical model, however, the switching lactose concentration cannot be obtained analytically, as discussed in Section 3.5. Therefore, this value was calculated numerically from optimal conditions 3.14 applied on model 5.6. Parameters for time-optimal control at $\Delta P = 20.2\,\text{bar}$ for the two models are listed in Tab. 5.5.

Table 5.5: Optimal conditions for the LF and the empirical model

model	c_1^* [kg m^{-3}]	α [1]
LF	141.4	1
empirical	79.6	1

To compare the LF and the empirical models, a case study was simulated and experimentally verified for both models. A solution with initial lactose and sodium chloride concentrations $c_1^{init} = 50\,\text{g/L}$ and $c_2^{init} = 10\,\text{g/L}$ respectively was concentrated and desalinated to final concentrations $c_1^f = 70\,\text{g/L}$ and $c_2^f = 3\,\text{g/L}$. These concentrations were chosen taking volume limitation[5] and constraints on concentrations[6] into account. Simulations for the first two stages—C and CVD modes—are shown in Figures 5.10 and 5.11 for respective models.

[5] Section 4.1.2
[6] Time-optimal strategy consisting of three steps (C, CVD and D modes) on page 11

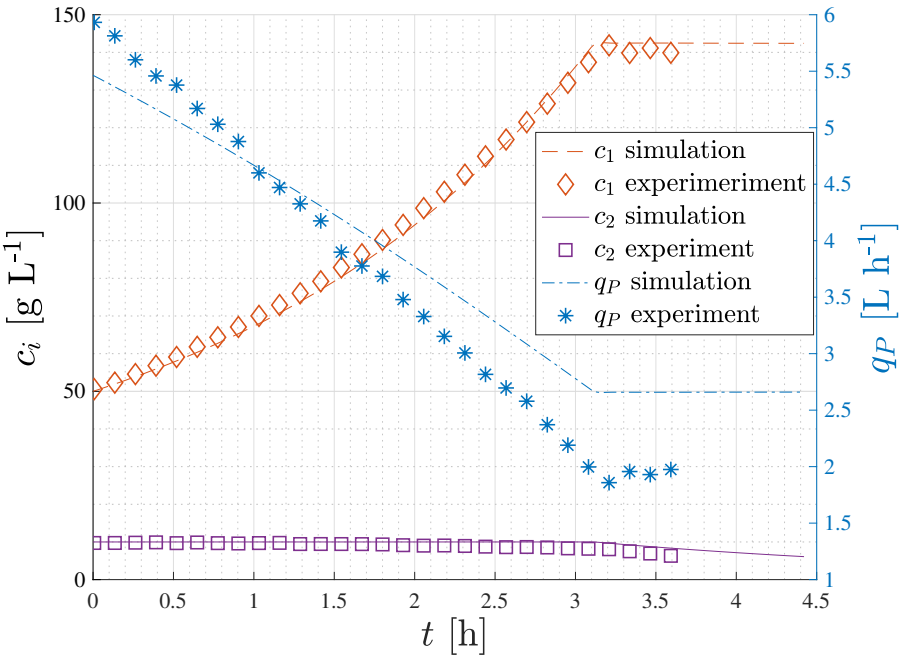

Figure 5.10: Case study of the limiting flux model, C and CVD modes

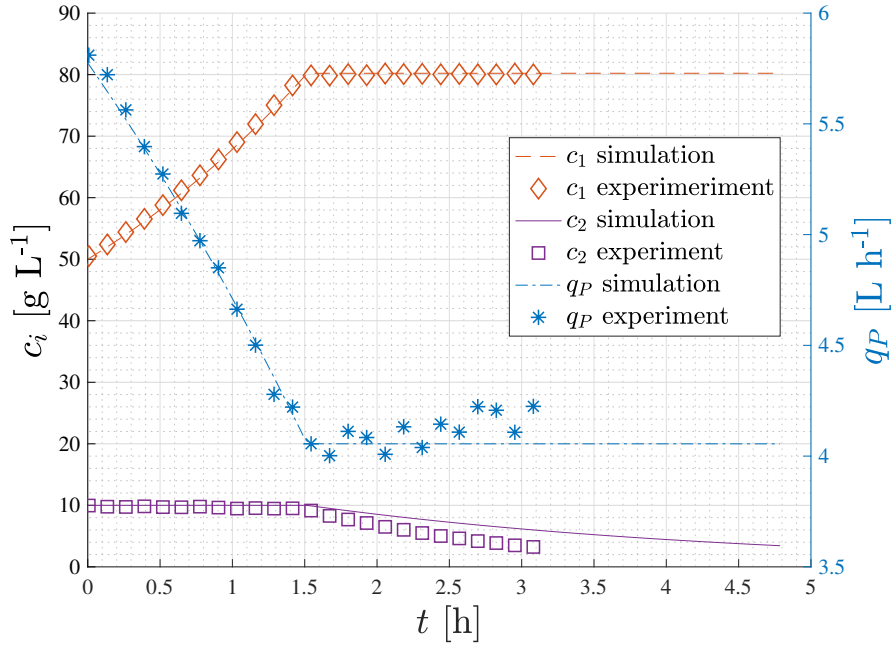

Figure 5.11: Case study of the empirical model, C and CVD modes

Comparison of overall filtration time, t_f, and water consumption (during the CVD mode), V_{CVD}, of traditional (non-optimal) strategy and optimal strategies for both models is shown in Table 5.6. While the traditional strategy consists of only two operation steps—C ($\alpha = 0$) and CVD ($\alpha = 1$)—the time-optimal strategy comprises also the D mode following overconcentration above desired concentration (as stated in Section 3.5). Time and water consumption in the form of percentage of the traditional strategy is Δt_f and ΔV_{CVD} respectively. It can be seen that optimal control for the empirical model achieved lower duration of the operation, though at more than sixfold higher water consumption during the CVD mode compared to the LF model. On the other hand, this water consumption is still lower than the consumption during the traditional strategy.

Table 5.6: Comparison of non-optimal and optimal strategies for the two models

	simulations				experiment	
α *strategy*	$\alpha = [0, 1]$		$\alpha = [0, 1, \infty]$		$\alpha = [0, 1, \infty]$	
model	emp.	LF	emp.	LF	emp.	LF
t_C [h]	1.12	1.15	1.58	3.14	1.46	3.16
t_{CVD} [h]	3.71	3.75	3.21	1.28	1.52	0.51
t_f [h]	4.83	4.90	4.79	4.42	2.98	3.67
V_{CVD} [L]	17.06	17.10	13.05	3.32	6.26	0.99
Δt_f[%]	100	100	99.17	90.20	61.98	74.90
ΔV_{CVD}[%]	100	100	76.49	19.42	36.69	5.79

As for the water-consumption optimal strategy, only a simulation for the LF model was executed with CVD at $c_1^* = 170.3\,\mathrm{kg\,m^{-3}}$ (lactose solubility at 22 °C according to [13] and Section 3.5) resulting in theoretical water consumption of $V_{CVD} = 1.85\,\mathrm{L}$ and total time of filtration $t_f = 4.46\,\mathrm{h}$. Comparable time result yet almost half of the water consumption relative to the strategy simulated for time-optimal LF diafiltration (column 5 in Table 5.6) both prove well-founded consideration of the water consumption optimality.

The water-optimal $V_{D,min}$ simulation for the LF model shown in Fig. 5.13, considers the switching concentration $c_1 = 170.3\,\mathrm{kg\,m^{-3}}$ being the lactose solubility, i.e. the maximum real concentration. For the empirical model, however, the positive values of the permeate flux are given by concentrations lower than the c coefficient ($c = 167.9\,\mathrm{kg\,m^{-3}}$). At the value of c, the permeate flux is limited to *zero* in accordance with the empirical model 5.6 and Fig. 5.9. Noticeably, this strategy would lead to infinite time of filtration for the empirical model with theoretically no switching point. The water-optimal strategy was not experimentally verified for practical reasons, since the switching concentration is in the area of maximum lactose solubility.

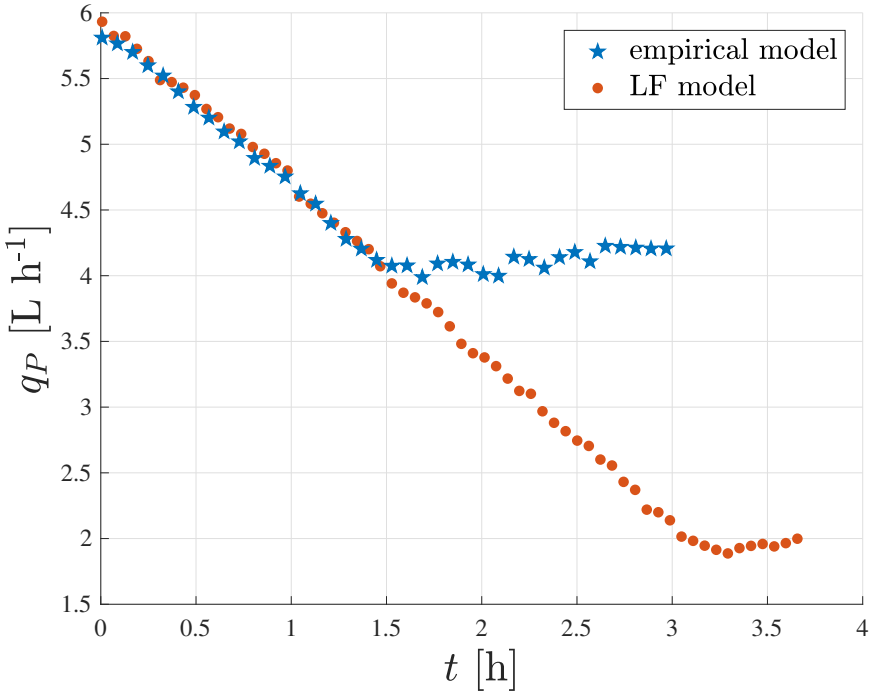

Figure 5.12: Permeate fluxes during both experiments

As it can be seen in Fig. 5.13, a significant difference from the previous theory occurs, as far as rejection of sodium chloride is concerned. Instead of rising of the c_2 value during the C phase, as it could be predicted by the process mass balance equations 3.13 with positive value of R_2 from Table 5.4, the concentration of salt decreases indicating negative value of rejection coefficient. Although specific mechanism of the negative rejection has not yet been sufficiently described, its presence has already been reported by authors relating this phenomenon to systems of charged membranes (NF) and single-charge ion electrolytes containing other components with high concentration and rejection coefficient [22], similarly to the system containing lactose and sodium chloride.

A possible explanation for not observing this in previous experiments, as indicated in Section 5.4, could be the fact that the concentration of lactose during the case study experiments was more than twice as high as the concentration during the R_2 estimations. To validate this assumption, further experiments at various range of lactose concentrations should be performed. Using eqn. 4.3, the rejection coefficient values during the case study filtrations are $R_2 = -0.1184$ and $R_2 = -0.1864$ respectively

employing the empirical and the limiting flux models.

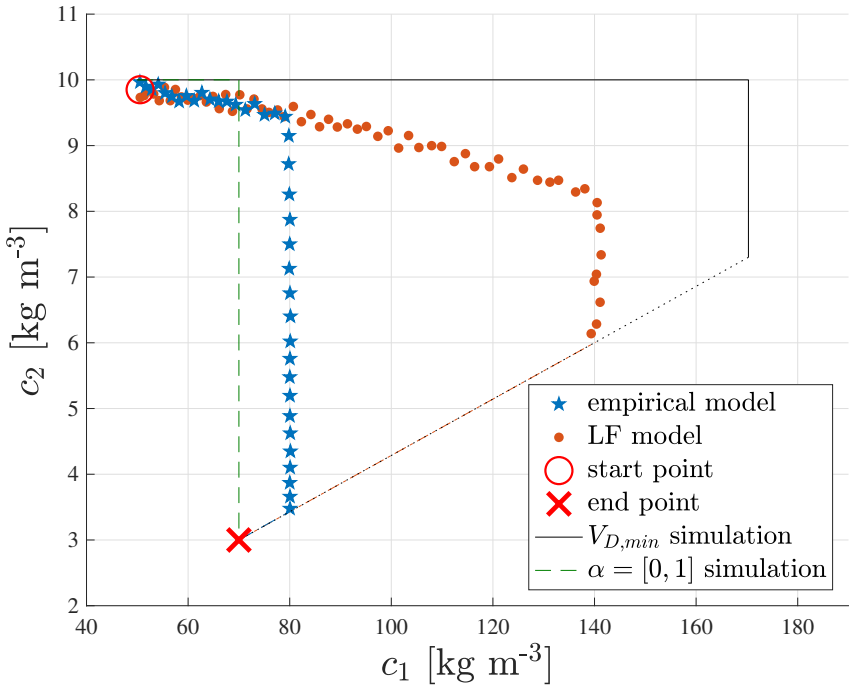

Figure 5.13: Concentration trajectory during non-optimal, water-optimal and time-optimal strategies for both experiments

A strong distinction between simulated and measured permeate flux in Fig. 5.10 is caused by inefficient data fitting of the LF model (see the wide confidence interval of the c_{lim} parameter in Table 5.1). Since the values of the two model parameters strongly influence the permeate flux, the variation would be minimised by providing an extra C mode experiment at same conditions as for the parameters estimation measurement. This feature of the model is, on the contrary, also an advantage regarding the possibility of an on-line parameter estimation. Furthermore, a smooth rise of the permeate flux during both experiments in the CVD mode, when only the salt concentration decreases, indicates a small yet non-negligible effect of the micro-solute on the permeate flux. This trend was not observed before since no data measurement in the CVD mode was provided.

Chapter 6

Conclusion

Modelling of the nanodiafiltration process was studied within the framework of modelling approaches used in the literature up to date. Nevertheless, specific mechanism (especially in such complex case of nanofiltration studied in this work) was not examined into particular depth. The membrane (considered as a *black box*) was thus observed in measurements tracking the influence of solutes concentrations and transmembrane pressure as input independent variables on the permeate flux as the output dependent variable.

For modelling of the permeate flux, two standard models were used—the limiting flux model and the generalised limiting flux model. Parameters of these models were estimated using non-linear least-squares regression of the mathematical models over the measured data in MATLAB 2017b.

Moreover, a new model was derived from an already existing empirical one. Building of this model constitutes a substantial part of this work. Coefficients of this model were determined in two steps. Firstly, specific concentration-dependent partial parameters of the model were analysed for the model design. Secondly, the coefficients of these concentration dependencies were evaluated also using non-linear regression. Eventually, a complete form of the empirical model was built with all coefficients established together in the second step.

Subsequently, parameters for optimal strategy were evaluated from related optimality conditions for the limiting flux model. For the empirical model, time-optimal parameters were determined numerically. The third model was excluded from the time-optimality inspection for its redundant micro-solute influence description. The two selected models were further examined in a case study.

In the case study, a solution containing lactose and sodium chloride was concentrated with respect to the sugar and diluted with respect to the salt. For both tested models of the permeate flux, the diafiltration strategy consisted of three following steps—concentration, constant-volume diafiltration and dilution. The optimality conditions of the case study were evaluated in accordance with appropriate equations. The traditional strategy consisting only of C and CVD modes was simulated and compared to the time-optimal one within each model. The comparison exhibited apparent

benefits in terms of both duration of the operation and water consumption.

Moreover, an experimental verification was executed to compare the time-optimal strategies proposed by the two models. While the strategy proposed for the limiting flux model showed lower water consumption during the experiment, the empirical model strategy provided shorter time of the overall process. Nevertheless, even the strategy based on the empirical model dominated over the traditional one also in terms of water consumption.

In order to investigate the optimal strategy for minimising water consumption, a simulation was made for the limiting flux model. It showed that, theoretically, this approach is comparably time-efficient to the time-optimal strategy, reducing water consumption almost by half. It was shown that for the empirical model, the solvent minimising condition would lead to infinitely long operation. For further analysis of the optimal strategies based on the economic balance, optimisation of the total profit of the process would be vital for evaluating its industrial viability.

During the case study measurements, the most significant variation of simulation from reality was observed in the constant-volume diafiltration mode for both models. This was caused by a strong difference in the real rejection coefficient value, leading to a notable decline in the sodium chloride concentration already during the concentration mode. Even though this phenomenon might act favourably for the overall process time minimisation, it introduced an error of the time estimation of more than 50% in the CVD mode for both models assuming no rejection of the salt by the membrane. This assumption is common within modelling of membrane processes other than nanofiltration. Based on this outcome, it was demonstrated that for modelling of the nanofiltration process, taking this effect into account is necessary. Observation of negative salt rejection was, however, not expected and would require further research of possible causes and scope.

Comparing the two permeate flux models, the main advantage of the empirical model over the limiting flux model is the possibility to use it directly for simulations, in which pressure-dependency of the permeate flux needs to be established. Such approach may be helpful e.g. in simulations of processes with considerable fouling, where constant performance of the permeate flux is required to be maintained by a continuous pressure profile change.

On the other hand, the limiting flux model benefits from its notable simplicity (two constant parameters) and could be used also for on-line parameters estimation of

processes with the optimal strategy evaluation *in situ* at constant pressure. Both parameters of this model are, however, assumed constant at given concentration range and at constant transmembrane pressure. This approach proved to be effective in the case study, with the parameters of this model, similarly to the empirical model parameters, developed in form more complex concentration- or flux-regime-functions in the literature.

A major drawback of both models is neglecting of the effect of other solutes, for example sodium chloride. This disadvantage was exhibited during the CVD regime of both models, when the decreasing salt concentration correlated with increasing permeate flux. This suggests their reliable use only in cases of low micro-solute concentrations, where the influence of other solutes on the permeate flux is indeed negligible. For detailed clarification of the micro-solute influence, experiments with larger sodium chloride concentrations should be done in non-recirculation configuration.

Furthermore, the impact of temperature was not studied in this work. This limits the estimated parameters (or the parameter estimation approach) only to a constant-temperature process. The effect of temperature on the model parameters should be investigated in further measurements at different thereof, expanding the proposed concentration- and pressure-dependent models also to a temperature-dependent one. For processes experiencing a temperature-changing profile, e.g. in fouling compensation via increasing temperature, this approach might prove useful.

Chapter 7

Resumé

Membránové separačné procesy, založené na rozdeľovaní zložiek tekutých zmesí selektívnym transportom cez membránu, sú jedným z najmodernejších a najefektívnejších spôsobov separácie v súčasnosti. V poslednej dobe nachádzajú svoje uplatnenie čoraz viac v predúprave vody, v spracovaní odpadových vôd, v regeneráciách organických rozpúšťadiel chemickej výroby, v potravinárskom a farmaceutickom priemysle pri spracovávaní tepelne labilných látok, ale aj v biochemickom priemysle v hybridných systémoch.

Do jednej zo spomenutých oblastí využitia membrán—potravinársky priemysel, patrí aj spracovanie mlieka resp. srvátky. Tá je totiž bohatým prírodným zdrojom laktózy, ktorá je pre svoje vhodné vlastnosti nachádza využívaná v iných priemyselných odvetviach, najmä v pekárenskom a farmaceutickom priemysle. Spracovanie srvátky pri výrobe laktózy sa mnohokrát nezaobíde bez membránového zakoncentrovania a parciálnej demineralizácie surového roztoku, na čo je výhodným riešením použitie nanofiltrácie ako jedného z najnovšie sa rozvíjajúcich druhov tlakových membránových procesov. Diafiltráciou ako sekvenciou viacerých operácií možno teda zakoncentrovať makrozložku a následne znížiť koncentráciu mikrozložky premývaním roztoku čistým rozpúšťadlom. Čo najúspornejší režim takéhoto procesu je z ekonomického hľadiska nutné zabezpečiť najmä optimalizáciou celkového času filtrácie a množstva čistého rozpúšťadla použitého na premývanie.

Nanofiltračná laboratórna stanica, ktorej schéma je na Obrázku 4.1, bola pri tejto práci použitá na experimentálne určovanie parametrov matematického modelu nanofiltrácie s diafiltračným zakoncentrovávaním a premývaním, pričom ako roztok na zakoncentrovanie bol použitý vodný roztok laktózy s chloridom sodným ako zložkou na vymytie zo zmesi. Pri matematickom modelovaní procesu boli zohľadnené celkovo tri rôzne modely toku *permeátu* (prúdu prechádzajúceho cez membránu) ako funkcie koncentrácie laktózy a cezmembránového tlaku. Tradičný model *limitujúceho toku* (známy tiež ako *gélový* model) 3.6 s jeho rozšírením na vplyv koncentrácie soli—modelom vo všeobecnom tvare 3.7, boli fitované na nameraných údajoch pre cezmembránový tlak $\Delta P = 20.2\,\mathrm{bar}$—vypočítané parametre modelov sú uvedené v Tabuľke 5.1.

Tretím modelom toku permeátu bol empiricky navrhnutý model 5.6 vychádzajúci z ex-

ponenciálneho empirického modelu v práci [18] pri zanedbateľnom zanášaní membrány. Návrh parametrov tohto modelu vo forme koncentračných závislostí bol vykonaný postupnou grafickou analýzou a nelineárnou regresiou na základe experimentov merania toku permeátu pri rôznych cezmembránových tlakoch pre roztoky s rôznymi koncentráciami laktózy a soli. Celkový tvar empirického modelu bol určený z čiastkových parametrov. Nelineárnou regresiou sa nakoniec znova určili koeficienty jednotlivých parametrov empirického modelu určeného vo forme explicitnej funkcie koncentrácie laktózy a cezmembránového tlaku. Hodnoty koeficientov sú uvedené v Tabuľke 5.3.

Dôležitou premennou pri modelovaní celkového procesu vo forme sústavy obyčajných diferenciálnych rovníc 3.13 je tzv. *zadržiavacia schopnosť* membrány (tiež *rejekčný* alebo *odporový* koeficient) definovaná vzťahom 3.5. Zatiaľ čo pre laktózu bola uvažovaná absolútna zádrž membránou ($R_1 = 1$), pre mikrozložku—soľ, bola vypočítaná z troch rôznych experimentov (uvedené hodnoty v Tabuľke 5.4). Pri experimentálnom overení prípadovej štúdie sa však zistilo, že koncentrácia laktózy vyššia ako pri experimentálnom zisťovaní samotnej hodnoty zádrže spôsobuje fenomén *zápornej zádrže*, ako o tom informuje práca [22]. Pre účely simulácie procesu v prípadovej štúdii bola preto uvažovaná hodnota zadržiavacej schopnosti membrány pre soľ nulová, aby sa demonštrovala výrazná odchýlka spôsobená bežne prijímaným zjednodušením, $R_2 = 0$, ktoré je teda pre daný prípad nanofiltrácie neprijateľné.

Na návrh časovo optimálnej prevádzky membránového procesu boli použité kriteriálne vzťahy 3.14 a 3.15 odvodené v práci [15]. Z vypočítaných parametrov modelu limitujúceho toku a empirického modelu boli pre tieto modely následne určené hodnoty veličín riadiacich optimálnu prevádzku uvedené v Tabuľke 5.5. Zovšeobecnený polarizačný model do optimalizácie zahrnutý nebol, pretože vplyv soli na tok permeátu v danom koncentračnom rozsahu sa v meraniach ukázal ako zanedbateľný.

Optimálne podmienky prevádzky boli následne otestované na prípadovej štúdii sledujúcej rozdielny prístup k optimálnej prevádzke procesu na základe rozdielnych modelov. Táto štúdia bola jednak simulovaná a následne aj experimentálne overená, pričom sa sledovalo zakoncentrovanie laktózy z 50 g/L na 70 g/L a zníženie koncentrácie soli z 10 g/L na 3 g/L. Časovo optimálna stratégia pre tento prípad diafiltrácie pozostáva z troch krokov—prekoncentrácie laktózy, diafiltrácie pri konštantnom objeme v systéme na požadovaný pomer konečných koncentrácií jednotlivých zložiek a následného zriedenia zmesi určitým množstvom čistého rozpúšťadla.

Simulácie optimálnych stratégií v prípadovej štúdii ukázali pozitívny vplyv časovej op-

timalizácie oproti bežnej stratégii pozostávajúcej len z dvoch krokov—zakoncentrovania laktózy na požadovanú hodnotu a diafiltrácie pri konštantnom objeme na požadované koncentrácie oboch zložiek. Grafické porovnanie simulácií pre jednotlivé trajektórie koncentrácií sú zhrnuté graficky na Obrázku 5.13. Na tomto obrázku teda tiež vidno spomenutý pokles koncentrácie soli vplyvom záporného odporového koeficienta, ktorý bol pre filtráciu podľa modelu limitujúceho toku vypočítaný na hodnotu $R_2 = -0.1864$, zatiaľ čo pre empirický model $R_2 = -0.1184$. Dôkladnejšiemu preskúmaniu *zápornej zádrže* membránou by bolo nutné venovať experimenty sledujúce napríklad vplyv koncentrácie laktózy na túto hodnotu.

Porovnanie simulácií s experimentálnymi výsledkami prípadovej štúdie je zase možné vidieť na Obrázku 5.10 pre model limitujúceho toku a na Obrázku 5.11 pre empirický model. Z týchto porovnaní vidno tiež odchýlku v oboch modeloch pre popis toku permeátu počas premývacieho režimu, čo naznačuje vplyv mikrozložky, ktorú ani jeden z modelov nezohľadňuje, keďže oba modely boli určené z meraní pre ustálené hodnoty toku permeátu. Zároveň sa ukázala prevádzka filtrácie podľa empirického modelu ako rýchlejšia v porovnaní s filtráciou podľa modelu limitujúceho toku, ako vidno na Obrázku 5.12. Tento model však na druhej strane dominoval oproti empirickému modelu menším množstvom spotrebovanej vody ako rozpúšťadla počas diafiltračného režimu. Oproti simulácií tradičných stratégií pre oba modely, obe stratégie navrhnuté pre optimalizáciu doby prevádzky sa ukázali ako výhodné z pohľadu jednak celkového času filtrácie aj spotreby vody.

Zhodnotenie optimalizácie procesu podľa minimalizácie spotreby rozpúšťadla neprinieslo porovnateľné závery. Kým v prípade modelu limitujúceho toku prepínacia koncentrácia laktózy je prakticky limitovaná jedine rozpustnosťou laktózy, simulovaná optimálna prevádzka podľa spotreby vody je značne výhodnejšia a porovnateľne dlhá ako v prípade optimalizácie podľa času. Na druhej strane optimalizáciu spotreby vody v prípade empirického modelu nebolo možné zhodnotiť, keďže pri prepínacej koncentrácii o niečo menšej ako rozpustnosť laktózy sa tok permeátu blíži k nule a takáto prevádzka by viedla k nekonečne dlhému procesu.

Pre ďalšie možnosti štúdia z hľadiska modelovania nanofiltračného procesu by mohlo byť vhodné najmä detailnejšie posúdenie vplyvu mikrozložky v porovnateľnom koncentračnom pomere k makrozložke, vplyv teploty na parametre jednotlivých modelov, ale tiež detailnejšie vyšetrenie zápornej rejekcie mikrozložky membránou. K celkovej optimalizácií procesu by prispelo posúdenie optimálnej prevádzky z hľadiska optimalizácie na báze celkovej ekonomickej bilancie prevádzky.

Bibliography

[1] Al Mamun, M. A., Bhattacharjee, S., Pernitsky, D., and Sadrzadeh, M. Colloidal fouling of nanofiltration membranes: Development of a standard operating procedure. *Membranes 7*, 1 (03 2017), 4.

[2] Bernauer, B., Bleha, M., Bouzek, K., Černín, A., Fíla, V., Friess, K., Izák, P., Jiránková, H., Kárászová, M., Kočiřík, M., Mikulášek, P., Novák, L., Paidar, M., Palatý, Z., Schauer, J., and Šípek, M. *Membránové procesy*. VŠCHT, Praha, 2012.

[3] Blatt, W. F., Dravid, A., Michaels, A. S., and Nelsen, L. *Solute Polarization and Cake Formation in Membrane Ultrafiltration: Causes, Consequences, and Control Techniques*. Springer US, Boston, MA, 1970, pp. 47–97.

[4] Dojčanský, J., and Longauer, J. *Chemické inžinierstvo II.* Malé Centrum, Bratislava, 2000.

[5] Goh, P., Lau, W., Othman, M., and Ismail, A. Membrane fouling in desalination and its mitigation strategies. *Desalination 425* (2018), 130 – 155.

[6] Hilal, N., Al-Zoubi, H., Darwish, N., Mohamma, A., and Arabi, M. A. A comprehensive review of nanofiltration membranes:treatment, pretreatment, modelling, and atomic force microscopy. *Desalination 170*, 3 (2004), 281 – 308.

[7] Hoogers, G. *Fuel cell technology handbook*. CRC Press, Boca Raton, 2003.

[8] Illanes, A. Chapter 1 - lactose: Production and upgrading. In *Lactose-Derived Prebiotics*, A. Illanes, , C. Guerrero, C. Vera, , L. Wilson, R. Conejeros, , and F. Scott, Eds. Academic Press, San Diego, 2016, pp. 1 – 33.

[9] Ma, S., Kassinos, S. C., and Kassinos, D. Direct simulation of the limiting flux: I. interpretation of the experimental results. *Journal of Membrane Science 337*, 1 (2009), 81 – 91.

[10] Marchetti, P., Jimenez Solomon, M. F., Szekely, G., and Livingston, A. G. Molecular separation with organic solvent nanofiltration: A critical review. *Chemical Reviews 114*, 21 (2014), 10735–10806. PMID: 25333504.

[11] McKay, M. D., Beckman, R. J., and Conover, W. J. A comparison of three methods for selecting values of input variables in the analysis of output from a computer code. *Technometrics 21*, 2 (1979), 239–245.

[12] Mulder, M. *Basic Principles of Membrane Technology*. Kluwer Academic Publishers, Dordrecht, 1991.

[13] Mullin, J. Appendix. In *Crystallization (4th Edition)*. Elsevier, 2001.

[14] Ng, C. Y., Mohammad, A. W., Ng, L. Y., and Jahim, J. M. Membrane fouling mechanisms during ultrafiltration of skimmed coconut milk. *Journal of Food Engineering 142* (2014), 190 – 200.

[15] Paulen, R., and Fikar, M. *Optimal Operation of Batch Membrane Processes*. Springer, Cham, 2016.

[16] Paulen, R., Jelemenský, M., Fikar, M., and Kovács, Z. Optimal balancing of temporal and buffer costs for ultrafiltration/diafiltration processes under limiting flux conditions. *Journal of Membrane Science 444* (2013), 87 – 95.

[17] Rajagopalan, N., and Cheryan, M. Process optimization in ultrafiltration: Flux-time considerations in the purification of macromolecules. *Chemical Engineering Communications 106*, 1 (1 1991), 57–69.

[18] Saltik, M. B., Özkan, L., Jacobs, M., and van der Padt, A. Dynamic modeling of ultrafiltration membranes for whey separation processes. *Computers & Chemical Engineering 99* (2017), 280 – 295.

[19] Sharma, A., Valo, R., Kalúz, M., Paulen, R., and Fikar, M. Experimental validation and comparison of time-optimal and industrial strategy for membrane separation process. In *Preprints of the 9th Vienna International Conference on Mathematical Modelling, Vienna, Austria, February 21-23, 2018* (2018), IFAC, pp. 869–874.

[20] Suárez, E., Lobo, A., Alvarez, S., Riera, F., and Álvarez, R. Demineralization of whey and milk ultrafiltration permeate by means of nanofiltration. *Desalination 241*, 1 (2009), 272 – 280. The Third Membrane Science and Technology Conference of Visegrad Countries (PERMEA); part 2.

[21] Wijmans, J., Nakao, S., and Smolders, C. Flux limitation in ultrafiltration: Osmotic pressure model and gel layer model. *Journal of Membrane Science 20*, 2 (1984), 115 – 124.

[22] Yaroshchuk, A. E. Negative rejection of ions in pressure-driven membrane processes. *Advances in Colloid and Interface Science 139*, 1 (2008), 150 – 173. Membrane Electrochemistry: Selected papers from the 33rd Conference on Membrane Electrochemistry, Russia, May 2007.